High performance photodetectors based on high quality InP nanowires*

Yan-Kun Yang(杨燕琨), Tie-Feng Yang(杨铁锋), Hong-Lai Li(李洪来), Zhao-Yang Qi(祁朝阳), Xin-Liang Chen(陈新亮), Wen-Qiang Wu(吴文强), Xue-Lu Hu(胡学鹿), Peng-Bin He(贺鹏斌), Ying Jiang(蒋英), Wei Hu(胡伟), Qing-Lin Zhang(张清林), Xiu-Juan Zhuang(庄秀娟), Xiao-Li Zhu(朱小莉)†, and An-Lian Pan(潘安练)‡

Key Laboratory for Micro-Nano Physics and Technology of Hunan Province, Key Laboratory for Micro/Nano Optoelectronic Devices of Ministry of Education, State Key Laboratory of Chemo/Biosensing and Chemometrics, School of Physics and Electronics Science, Hunan University, Changsha 410082, *China*

(Received 11 August 2016; revised manuscript received 10 September 2016; published online 30 September 2016)

In this paper, small diameter InP nanowires with high crystal quality were synthesized through a chemical vapor deposition method. Benefitting from the high crystallinity and large specific surface area of InP nanowires, the simply constructed photodetector demonstrates a high responsivity of up to 1170 $A \cdot W^{-1}$ and an external quantum efficiency of 2.8×10^5% with a fast rise time of 110 ms and a fall time of 130 ms, even at low bias of 0.1 V. The effect of back-gate voltage on photoresponse of the device was systematically investigated, confirming that the photocurrent dominates over thermionic and tunneling currents in the whole operation. A mechanism based on energy band theory at the junction between metal and semiconductor was proposed to explain the back-gate voltage dependent performance of the photodetectors. These convincing results indicate that fine InP nanowires will have a brilliant future in smart optoelectronics.

Keywords: InP nanowires, small diameter, photodetector, back-gate voltage

PACS: 81.07.Gf, 85.60.Gz **DOI:** 10.1088/1674-1056/25/11/118106

1. Introduction

It is generally known that one-dimensional (1D) semiconductor nanostructures are ideal systems for exploring basic physical properties at the nanoscale, such as quantum conductance, ballistic conduction, transformations and low thermal conductivity, which are of great importance for applications in nanophotonics and nanoelectronics.[1–5] More interestingly, when the sizes of such semiconductor structures diminish further, the resulting leap of specific surface area makes them much more sensitive and efficient for probing the surface chemical processes and optical signals around, as compared with their thicker counterparts which can significantly improve the performances of present chemical/biosensors and photodetective devices.[6–8] For instance, Hu *et al.* recently certified that the large specific surface area of small diameter SnO_2 nanowires (NWs) can boosts the efficiency of the photodetectors.[9] Inspired by these virtues, the interest of developing small-sized 1D semiconductor nanomaterials has been culminated in the past few years.[10–12]

As a vital III–V semiconductor, 1D Indium Phosphide (InP) has demonstrated wide applications in electronic and optoelectronic fields for its natural merits, such as high carrier mobility, very low surface recombination velocity, and long carrier lifetime at room temperature.[13–16] Specially, this interesting material possesses a proper direct bandgap of 1.34 eV, which is proposed to be an attractive candidate for detecting visible radiation. Although many efforts have been devoted to the synthesis of 1D InP nanostructures systematically photoresponse investigations to date based on them are still limited.[17–20] More regrettably, the present works are generally focused upon the InP nanostructures of relatively large size, which did not allow full play to the advantages of 1D InP nanostructures in the photodetective field. Therefore, it is still highly desirable to develop high performance InP photodetectors based on the small-sized 1D nanostructures and conduct a comprehensive study of their working behaviors. In this work, small diameter InP NWs with high crystal quality and optical performances were successfully grown by a chemical vapor deposition (CVD) method, and field-effect transistors based on these individual InP NWs were built to study their electrical transport and photodetective properties. Benefitting from the high crystal quality and small diameter features of the NWs, a photodetector on the two-terminal configuration exhibited low power consumption and excellent light photoresponse, and the back-gate voltage dependent performance of the photodetectors was systematically investigated and explained using theoretical models. These succinct and high efficiency devices can expand the building blocks for high performance optoelectronic devices.

*Project supported by the National Natural Science Foundation of China (Grant Nos. 51525202, 61574054, 61505051, and 61474040), the Science and Technology Plan of Hunan Province, China (Grant Nos. 2014FJ2001 and 2014TT1004), and the Aid Program for Science and Technology Innovative Research Team in Higher Educational Institutions of Hunan Province, China.

†Corresponding author. E-mail: zhuxiaoli@hnu.edu.cn

‡Corresponding author. E-mail: anlian.pan@hnu.edu.cn

© 2016 Chinese Physical Society and IOP Publishing Ltd

2. Experiments

For the growth of small diameter InP nanowire, the moving source CVD method was used (the experimental setup is shown in Fig. A1 in Appendix A). Typically, an alumina boat filled with 0.05 g InP powder (Alfa Aesar, 99.9999%) was first placed upstream and far enough from the center of the furnace, and several silicon wafers coated with 3 nm thick gold film were placed downstream at the deposition area. Before heating, Ar/H_2 (15%) gas was introduced into the system at a rate of 50 sccm for 1 h, and the pressure was maintained at 3 Torr. The furnace was then heated to 780 °C (the substrate temperature was about 485 °C) for 3 mins to generate gold particles that served as catalysts for the growth of InP NWs. Then the boat with InP powder was shifted to the center of the furnace by a step motor. After 30 mins of growth, the furnace was naturally cooled down to room temperature. The as-grown NWs were characterized utilizing field emission scanning electron microscope (FE-SEM, Zeiss sigma-HD), atomic force microscopy (AFM, Brucker Bioscope System), x-ray diffraction (XRD) (Rigaku D/Max 2500) and a transmission electron microscopy (TEM, Tecai F20) equipped with energy-dispersive x-ray spectroscopy (EDX). Micro-photoluminescence (μ-PL) and Raman scattering spectra were carried out on a laser confocal Raman spectrometer (LABRAM-010, France) coupled with a continuous 632.8 nm laser for excitation.

Back-gate single NW field-effect transistors (FETs) were then fabricated. The as-obtained NWs were first dispersed in alcohol and then drop-cast onto the P^+-Si/SiO_2 (300 nm) wafers Cr/Au source and drain electrodes (5/65 nm) were defined by electron-beam lithography, metallization and lift-off process. The electrical transport measurements of FETs were conducted by the probe station combined with a semiconductor parameter analyzer (Keithley 4200-SCS). For photoresponse measurements, a power-tunable 520 nm semiconductor laser was used to provide incident light, while the time-dependent photocurrent were monitored by a current meter after switching on-off the illumination with a light chopper. All the measurements were conducted in air at room temperature.

3. Results and discussion

3.1. Morphology and structure characterization

As demonstrated by a typical SEM image (Fig. 1(a)), large quantities of InP NWs with a length of about 50–80 μm were achieved on the substrate. Basically, the NWs have small diameters of 29.1 ± 8.3 nm, based on AFM studies (Fig. A2), suggesting a large specific surface area of the NWs. XRD pattern of the product (Fig. 1(b)) was indexed to the zinc blende (ZB) crystal (JCPDS: 65-233) without any detectable wurtzite (WZ) phase. A TEM image of a typical InP NW in Fig. 1(c) shows smooth sidewall and uniform diameter of about 25 nm along its entire length with a Au particle at the tip, indicating the vapor–liquid–solid growth mechanism.[21,22] The corresponding EDX spectrum inserted in Fig. 3(c) reveals that the NW consists of elements In and P with an equal ratio, very close to the stoichiometric value for a InP compound. Figure 1(d) represents a high-resolution TEM image recorded along the [112] zone axis. This image with the selected area electron diffraction (SAED) pattern inserted documents the high single-crystal quality with the ZB structure of our sample, and its growth direction is [111], which is consistent with the literature.[23]

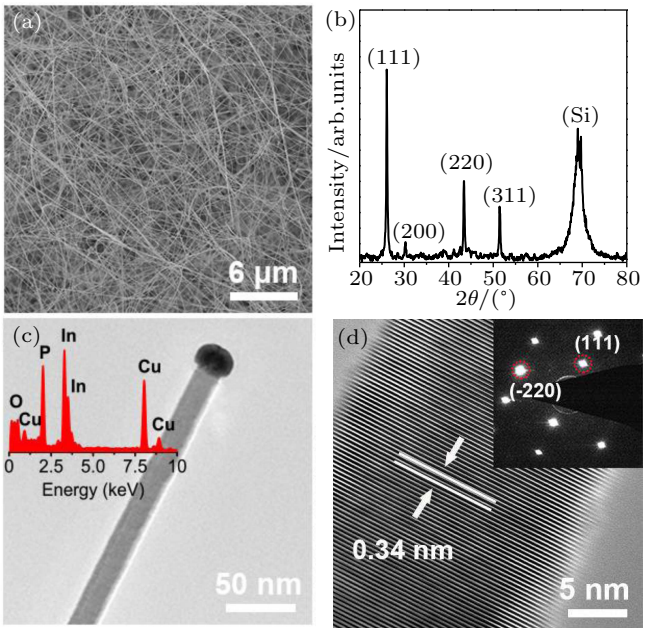


Fig. 1. (color online) (a) Typical SEM image of numerous InP NWs. (b) XRD pattern of the as-grown NWs. (c) TEM image and EDX spectrum of a single InP NW. (d) The corresponding HRTEM image together with the SAED pattern of the InP NW.

3.2. Optical and electronic properties

To further investigate the nature of InP NWs, optical characterizations were performed. A typical PL spectrum recorded from a single NW in Fig. 2(a) shows the emission peak located at 870 nm (∼ 1.42 eV), indicating a blue-shift of 50 nm compared with the bulk ZB InP PL (920 nm), which is much more moderate with respect to the defects related emission.[24] This blue-shift can be explained by quantum confinement effect[25] correlated well with the average diameter of our samples. Figure 2(b) shows the first-order Raman scattering spectrum of a single InP NW. By means of Lorentzian fitting, the two strong peaks observed can be associated with the transverse optical (TO) mode at 301 cm^{-1} and the longitudinal optical (LO) mode at 339 cm^{-1}. Comparing with the TO and LO modes of bulk InP, the detected modes in our nanostructure have 2 cm^{-1} and 6 cm^{-1} downshifts, respectively, which is ascribed to the quantum confinement effect as well.[26] In addition, the weak peak at 326 cm^{-1} probably originates from the surface optical (SO) mode as a consequence of fine size of the InP NW.[26]

These results further confirm the high quality and the large specific surface area characteristics of the achieved InP NWs.

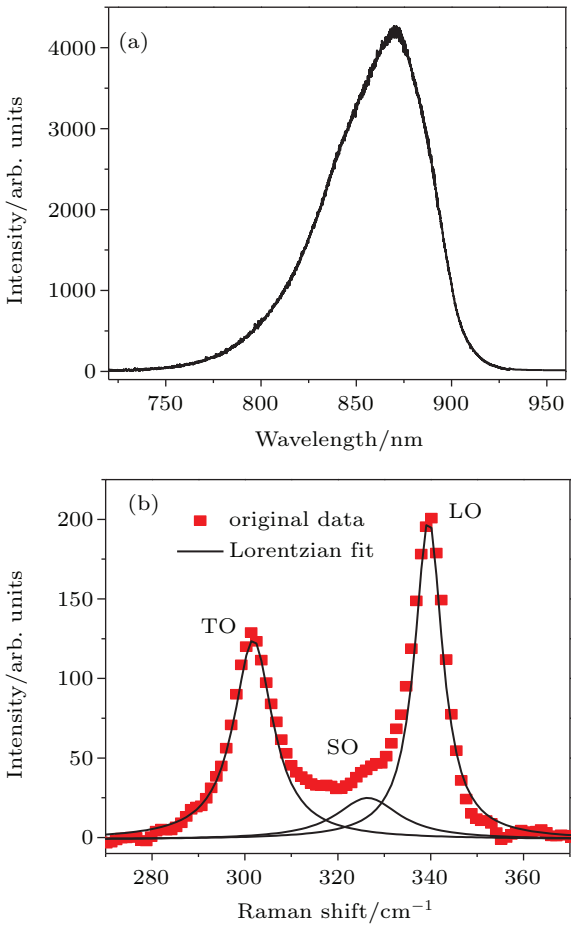


Fig. 2. (color online) (a) and (b) Typical μ-PL and Raman spectra of the as-grown InP NW excited with a 632.8 nm laser.

As illustrated in Fig. 3(a), back-gate single NW FETs were assembled to assess the electronic transport properties of the samples. Figure 3(b) shows the output characteristics of a representative device with a NW diameter of 30 nm and a channel length of 5.2 μm between two adjacent electrodes (a SEM image is shown in Fig. 3(a)). With the back-gate voltage (V_{GS}) rising from −10 V to 10 V, the conductance of the device gradually increases, revealing a good gate-dependence. Meanwhile, the transfer characteristics were investigated at a low drain bias (V_{DS}) of 0.1 V. As depicted in Fig. 3(c), the drain current (I_{DS}) increases when the V_{GS} mounts up, demonstrating a typical n-type semiconducting nature of the NWs, which is in agreement with the result observed by Hui *et al.*[27] In this study, the electron mobility μ_e of InP channel was derived from the transfer curve via the following formula:[28]

$$\mu_e = \frac{dI_{DS}}{dV_{GS}} \frac{L^2}{V_{DS}} \frac{\ln(4h/d)}{2\pi\varepsilon_r\varepsilon_0 L}, \quad (1)$$

where $dI_{DS}/(dV_{GS})$ refers to the transconductance of the device, the value is calculated to be around 12 nS, L is the channel length, h (300 nm) and d (30 nm) are the thicknesses of the dielectric SiO_2 layer and the NW diameter, ε_r is the relative dielectric constant of SiO_2 and ε is the permittivity of free space, respectively. As a result, the electron mobility was found to be 105 cm^2·V^{-1}·s^{-1}, which is comparable with the previous results.[20,27]

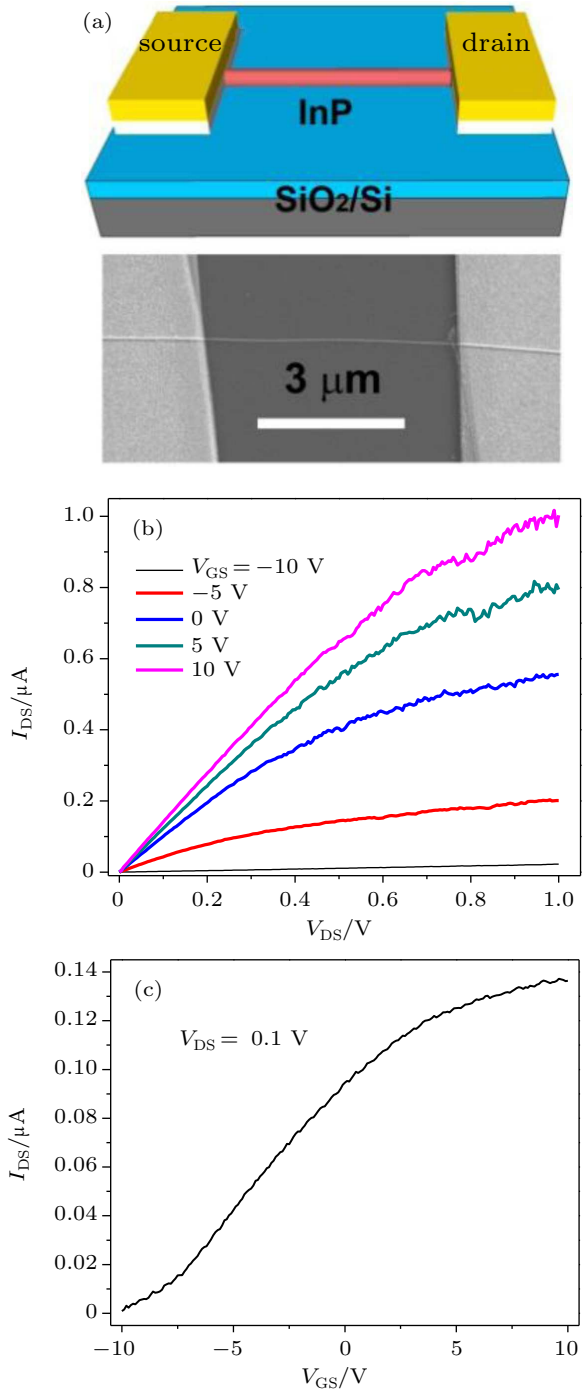


Fig. 3. (color online) (a) Schematic and SEM image of a back-gate single NW FET. (b) Output characteristics of the device at various V_{GS}. (c) Transfer curves measured at V_{DS} of 0.1 V.

3.3. Photoresponse performances

Benefitting from the high mobility, the InP NWs can in principle be available for high performance photodetectors. We first measured its photoresponse properties under V_{DS} =

0.1 V and $V_{GS} = 0$ V on the two-terminal structure as displayed in Fig. 4(a) by turning 520 nm laser illumination with different power intensities ranging from to 103.1 mW/cm^2. It can be observed that the drain current increases with the increased voltage, at the same time, it increases apparently with the increased light intensities. The spectral responsivity (R_λ) and external quantum efficiency (EQE) of the device can then be obtained by the following equations[29,30] $R_\lambda = I_{ph}/PS$ and EQE $= R_\lambda hc/e\lambda$, where I_{ph} represents the photocurrent defined as the difference between light current and dark current ($V_{DS} = 0.1$ V and $V_{GS} = 0$ V), P and S (0.156 μm^2) describe the corresponding light intensity and the effective illuminated area of the device, h refers to the Plank's constant, c is the velocity of light, e is the electronic charge and λ is the incident light wavelength, respectively. An outstanding responsivity value of up to 2200 A·W^{-1} can be obtained at the intensity of 4.64 mW/cm^2, although it trends a little downward when the laser intensity increases, the value of 1170 A·W^{-1} is still pretty high even at 103.1 mW/cm^2, indicating an excellent conversion ability of optical to electrical signals and a low power consumption of the device (Fig. 4(b)). In addition, the achievable EQE value was estimated to be 2.80×10^5% that can rival or even surpass the previous results.[17–20]

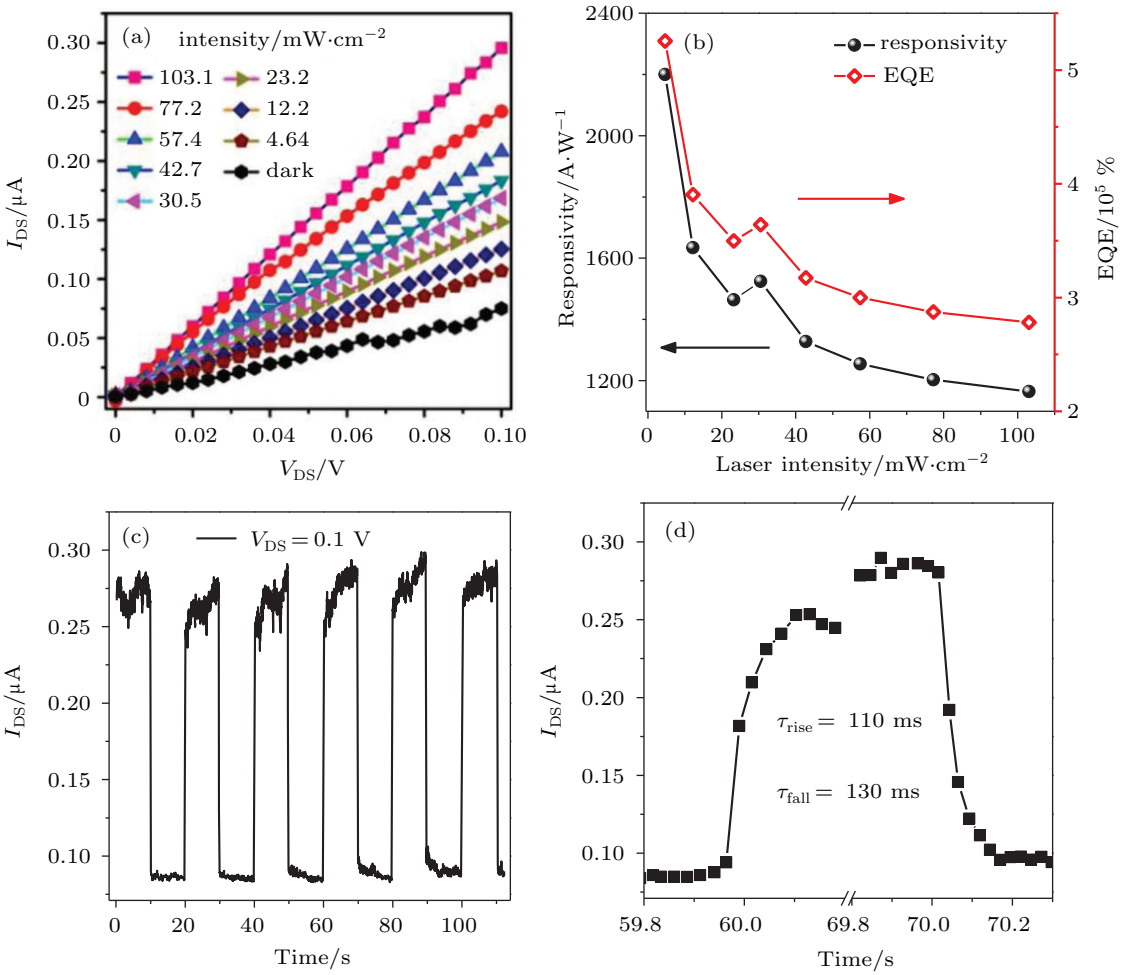


Fig. 4. (color online) (a) The I–V plots of the device in the dark and under 520 nm laser at different illumination intensities. (b) Responsivity and calculated EQE versus laser intensity at $V_{DS} = 0.1$ V and $V_{GS} = 0$ V. (c) Time-resolved switching behavior of the device under laser intensity of 103.1 mW/cm^2 at $V_{DS} = 0.1$ V. (d) Enlarged rise and fall sides over circle of 60–70 s.

To explore the capability of the photodetector for fast-varying optical signals, the time-response cycles of the device were obtained by periodically turning on and off the laser at 10 s intervals, under incident laser intensity of 103.1 mW/cm^2 at $V_{DS} = 0.1$ V and $V_{GS} = 0$ V. As plotted in Fig. 4(c), the device current rises up sharply and reaches to a steady state about 0.27 μA once the laser opened, and then falls down quickly to 0.08 μA when the light is blanked, demonstrating an excellent stability and reversible switching properties of the device. This good performance is confirmed by the longer-periodic time photoresponse measurements in Fig. A3. The rise time (τ_r) and fall time (τ_f), defined as the required time for the current rising to 90% and falling to 10% of the peak value, are about 110 ms and 130 ms, respectively, based on the enlarged curve in Fig. 4(d), which have comparability to the values improved by the ferroelectric-enhancing technique.[31] These good properties (both responsivity and response speed) are particularly attractive merits for optoelectronics and proba-

bly result from two unique characteristics of our NW samples. (i) The superior crystal quality. InP NWs with few defects benefit the transport of the carriers, thus increasing the photoconductive gain and facilitating the photocurrent to reach a steady state rapidly in both the rise and fall processes.[32,33] (ii) The small diameter of the NW ($\sim$ 30 nm). On the one hand, the chemisorption around the NW becomes prominent as a result of the large specific surface area arising from its tiny structure. Consequently, adsorbates attached on the NW surface as hole-traps would prolong the lifetime of photo-generated carriers,[34] which guarantees the high photo-gain and responsivity of our device when light is turned on. On the other hand, as light is turned off, defects and dangling bonds at the NW surface could increase the recombination rate of carriers, meaning a shorter fall time.[35] In fact, both high responsivity and fast response speed imply that the surface trapping and recombination relaxation reach an equilibrium for the semiconductor channel.[36]

3.4. Effect of gate voltage on photoresponse

Afterwards, we studied the effect of back-gate voltage on the performance of InP photodetectors. Figure 5(a) illustrates the plots of I_{DS} versus V_{GS} ($V_{DS} = 0.1$ V) under different laser intensities as before. The conductivity of InP channel under illumination in both OFF and ON states increases effectively across the whole gate voltage range employed, indicating that photocurrent dominates over thermionic and tunneling currents across the entire operating range of gate voltages. Figure 5(b) plots the photocurrents with different V_{GS} extracted from the transfer characterizations. Fitting the plots with power law of $I_{ph} \sim P^{\theta}$,[35] we can extract the factor θ determining the efficiency of the photo-generated charges to light intensity as a function of V_{GS} (-10 V to 10 V). At a low gate voltage of -10 V, a linear increase ($\theta = 0.98$) of the photocurrent with the light intensity confirms that the photocurrent is solely determined by the amount of photo-generated carriers.[37] Whereas, when the gate bias further increases from -10 to 10 V at interval of 5 V, the device puts up a sublinear behavior, that is, the factor θ decreases monotonously with different values of 0.98, 0.92, 0.82, 0.74, and 0.65. The sublinear relation between the photocurrent and the laser intensity may relate to a complex photocurrent-generated mechanism.[34,35] Figure 5(c) shows the responsivity and EQE recorded as a function of gate voltage under illumination intensity of 103.1 mW/cm^2 at 0.1 V bias, respectively. Similar to the modulation of channel conductivity, the gate voltage can bring a variation to the responsivity and EQE of InP photodetector. The responsivity of the device is only 138 A·W^{-1} when $V_{GS} = -10$ V, while V_{GS} sweeping to 10 V, a preeminent value up to 1436 A·W^{-1} can be achieved and the EQE also increases by an order of magnitude. This gate-tunable property can provide the potential for the pixelated imaging applications.[38]

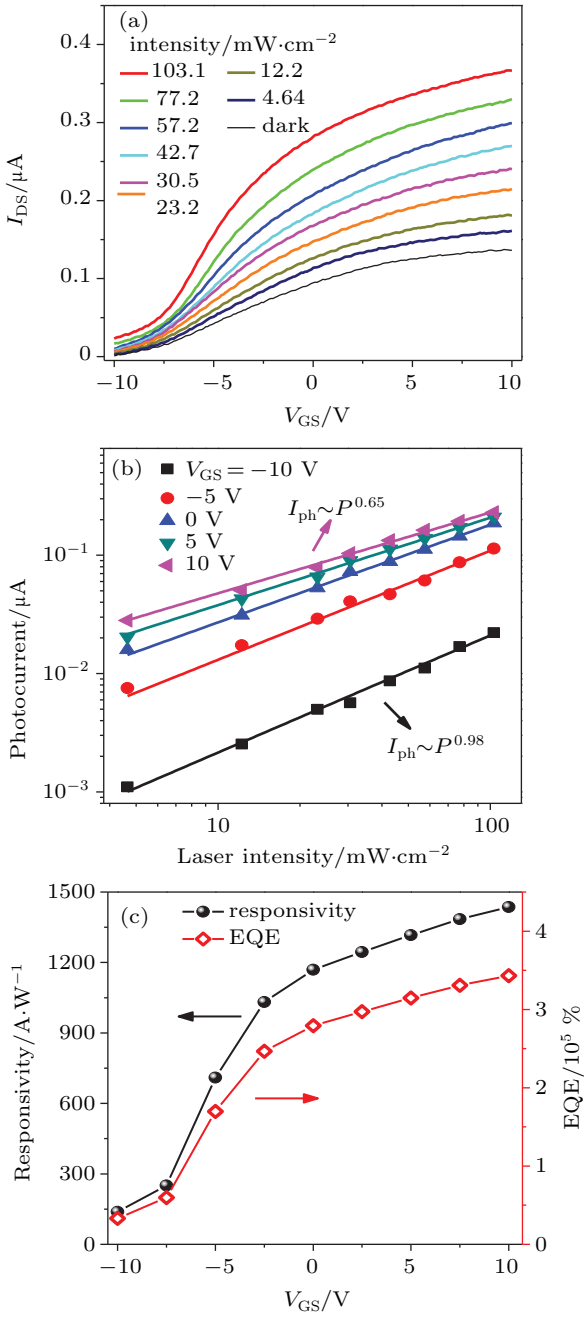


Fig. 5. (color online) (a) Plots of I_{DS} versus V_{GS} ($V_{DS} = 0.1$ V) under different laser intensities. (b) Relationship between photocurrent and laser intensity at various V_{GS}. The curves are fitted by the power law. (c) Responsivity and calculated EQE as a function of V_{GS} recorded at $V_{DS} = 0.1$ V under laser intensity of 103.1 mW/cm^2, respectively.

The above observed behaviors of our InP NW photodetectors can be explicated by a simple energy band diagram as depicted in Fig. 6.[31] As shown in Fig. 6(a), the InP device is in its quasi-equilibrium state under bias and illumination without back-gate voltage applied, which can be characterized by a small Schottky barrier at the interface between metal and semiconductor, where band tail drags especially slowly and depletion region extends deep into the channel.[39] When a negative gate voltage is applied, a larger barrier between InP and metal electrode occurs as compared to the state at zero gate voltage, hindering photo-generated carriers extrac-

tion by the applied bias voltage, thus leading to a low responsivity (Fig. 6(b)). Fortunately, since the width of depletion region can expand further with Schottky barrier increasing, the resulting strong local electric field in the semiconductor can separate the electron–hole pairs effectively, which guarantees a good dependence of the photocurrent.[40,41] At an extreme, the device photocurrent in the OFF state is merely determined by the photo-excited process and easily follows the linear relation to illumination intensity as described before in Fig. 5(b). Inversely, if the applied gate voltage is positive, the Schottky barrier can be lower, allowing more efficient photoresponse for the device (Fig. 6(c)).[42] However, the narrow depletion region cannot separate the electron–hole pairs effectively, which consequently easily deviate the relationship between photocurrent and illumination intensity from linear to sublinear dependence.

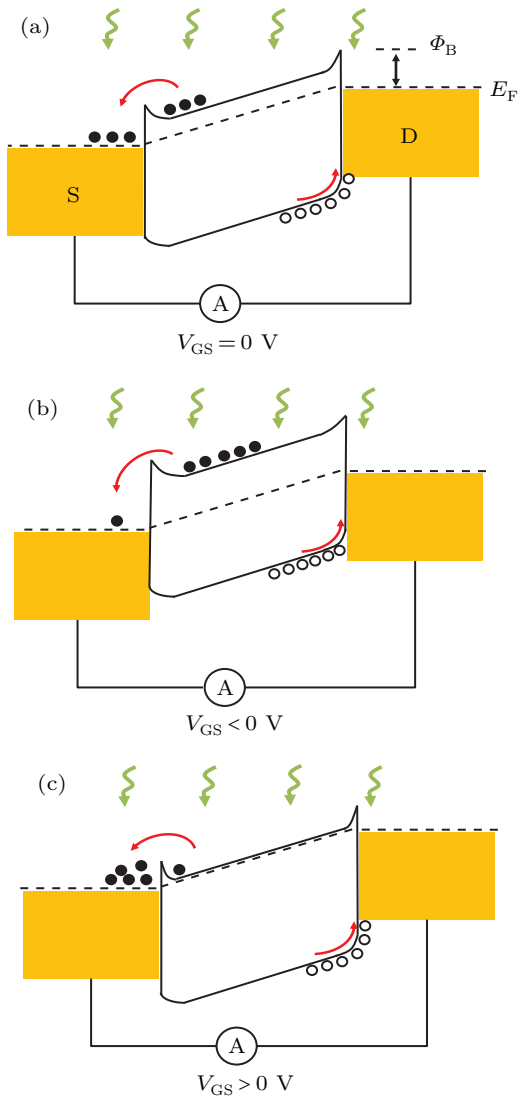


Fig. 6. (color online) Band diagrams of InP photodetector under bias and illumination when different gate voltages were applied: (a) $V_{GS} = 0$ V; (b) $V_{GS} < 0$ V and (c) $V_{GS} > 0$ V. The E_F is the new quasi-Fermi level and Φ_B is the Schottky barrier height. The full dots and the empty dots represent the photo-generated electrons and holes, respectively.

4. Conclusion

In summary, we have realized the synthesis of small diameter (less than 30 nm) and high crystallinity InP NWs that possess excellent optical properties. Electrical transport measurements of the nanostructures show a high electron mobility of 105 $cm^2 \cdot V^{-1} \cdot s^{-1}$. Benefitting from large specific surface area and high crystallinity character of the NWs, the as-fabricated photodetector exhibits good sensing performance, such as a responsivity of 1170 $A \cdot W^{-1}$, external quantum efficiency of $2.8 \times 10^5\%$ and fast response speed ($\tau_r = 110$ ms, $\tau_f = 130$ ms). In addition, the back-gate voltage related photoresponse of the device was investigated, which can be explicated by a simple energy band diagram. These findings may accelerate the progress of a new generation of optoelectronic devices.

Appendix A

Figure A1 shows the experimental setup for the synthesis of the InP NWs, figure A2 shows AFM studies of the InP NWs dispersed on a SiO_2 substrate, and the longer-periodic time photoresponse measurements of the device under laser intensity of 103.1 mW/cm^2 at $V_{DS} = 0.1$ V are shown in Fig. A3.

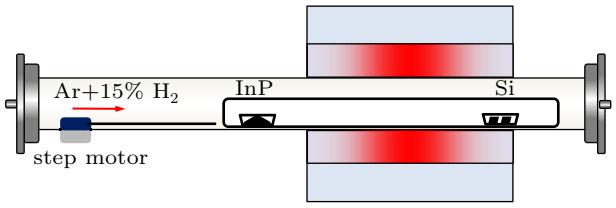


Fig. A1. (color online) Schematic diagram of the experimental setup for the synthesis of the InP NWs.

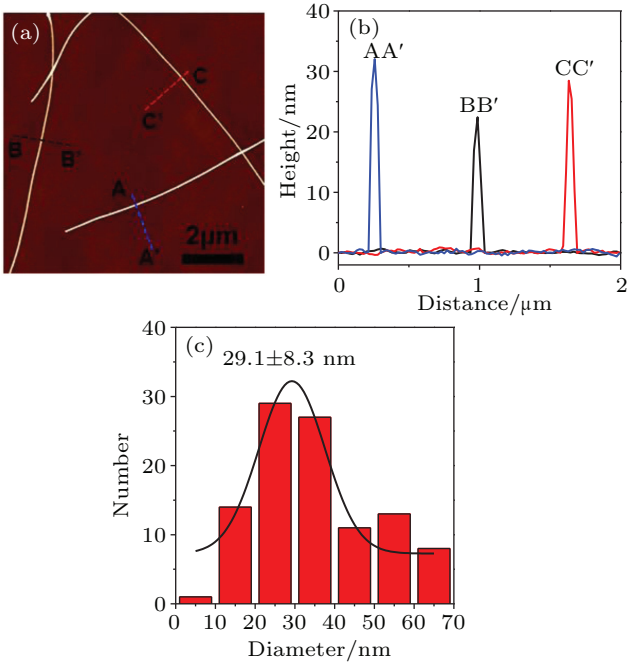


Fig. A2. (color online) (a) Contact-mode AFM height image of InP NWs dispersed on a SiO_2 substrate. (b) Representative cross sections taken along the lines in panel (a). (c) Diameter distribution of 100 individual NWs. Black wire refers to the corresponding Gaussian fit.

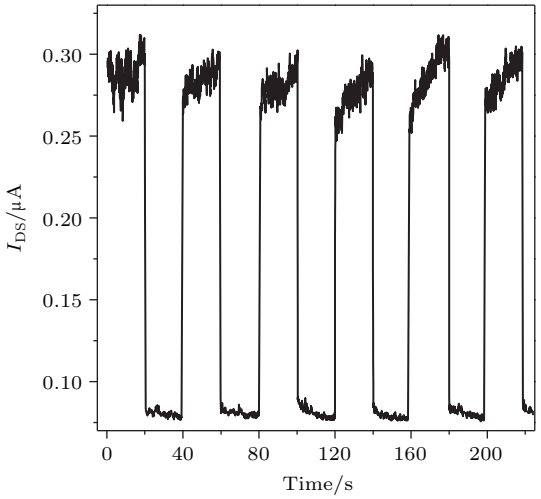


Fig. A3. The longer-periodic time photoresponse measurements of the device under laser intensity of 103.1 mW/cm^2 at $V_{DS} = 0.1$ V.

References

[1] Xu X X and Wang X 2009 *Inorg. Chem.* **48** 3890
[2] Zhao X, Wei C M, Yang L and Chou M Y 2004 *Phys. Rev. Lett.* **92** 236805
[3] Hochbaum A I, Chen R K, Delgado R D, Liang W J, Garnett E C, Najarian M, Majumdar A and Yang P D 2008 *Natrue* **451** 163
[4] Ren P Y, Zhu X L, Han J Y, Xu J Y, Ma L, Li H L, Zhuang X J, Zhou H, Zhang Q L, Xia M G and Pan A L 2014 *Nano-Micro Lett.* **6** 301
[5] Liu R B, Zhuang X J, Xu J Y, Li D B, Zhang Q L, Ding K, He P B, Ning C Z, Zou B S and Pan A L 2011 *Appl. Phys. Lett.* **99** 263101
[6] Cademartiri L and Ozin G A 2009 *Adv. Mater.* **21** 1013
[7] Wang D F, Liang J R, Li C Q, Yan W J and Hu M 2016 *Chin. Phys. B* **25** 028102
[8] Guo S, Li Z H, Song G L, Zou B S, Wang X X and Liu R B 2015 *J. Alloys Compd.* **649** 793
[9] Hu L F, Yan J, Liao M Y, Wu L M and Fang X S 2011 *Small* **7** 1012
[10] Shen G Z, Liang B, Wang X F, Huang H T, Chen D and Wang Z L 2011 *ACS Nano* **5** 6148
[11] Yang Z X, Han N, Fang M, Lin H, Cheung H Y, Yip S P, Wang E J, Hung T F, Wong C Y and Ho J C 2014 *Nat. Commun.* **5** 5249
[12] Duan X F and Lieber C M 2000 *Adv. Mater.* **12** 298
[13] Joyce H J, Wong-Leung J, Yong C K, Docherty C J, Paiman S, Gao Q, Tan H H, Jagadish C, Lloyd-Hughes J, Herz L M and Johnston M B 2012 *Nano Lett.* **12** 5325
[14] Duan X F, Huang Y, Cui Y, Wang J F and Lieber C M 2001 *Nature* **409** 66
[15] Wang J F, Gudiksen M S, Duan X F, Cui Y and Lieber C M 2001 *Science* **293** 1455
[16] Wallentin J, Anttu N, Asoli D, Huffman M, Aberg I, Magnusson M H, Siefer G, Fuss-Kailuweit P, Dimroth F, Witzigmann B, Xu H Q, Samuelson L, Deppert K and Borgström M T 2013 *Science* **339** 1057
[17] Chen G, Liang B, Liu Z, Yu G, Xie X M, Luo T, Xie Z, Chen D, Zhu M Q and Shen G Z 2014 *J. Mater. Chem. C* **2** 1270
[18] Sarkar A, Logeeswaran V J, Kobayashi N P, Straznicky J, Wang S Y, Williams R S and Islam M S 2007 *Proc. SPIE* **6768** 67680P
[19] Logeeswaran V J, Oh J, Nayak A P, Katzenmeyer A M, Gilchrist K H, Grego S, Kobayashi N P, Wang S Y, Talin A A, Dhar N K and Islam M S 2011 *IEEE J. Sel. Top. Quant.* **17** 1002
[20] Duan T Y, Liao C N, Chen T, Yu N, Liu Y, Yin H, Xiong Z J and Zhu M Q 2015 *Nano Energy* **15** 293
[21] Wagner R S and Ellis W C 1964 *Appl. Phys. Lett.* **4** 89
[22] Xing Y J, Yu D P, Xi Z H and Xue Z Q 2002 *Chin. Phys. B* **11** 1047
[23] Liu C, Dai L, You L P, Xu W J and Qin G G 2008 *Nanotechnology* **19** 465203
[24] Shen G Z, Bando Y, Liu B D, Tang C C and Golberg D 2006 *J. Phys. Chem. B* **110** 20129
[25] Gudiksen M S, Wang J F and Lieber C M 2002 *J. Phys. Chem. B* **106** 4036
[26] Ren P Y, Xu J Y, Wang Y C, Zhuang X J, Zhang Q L, Zhou H, Wan Q, Shan Z P, Zhu X L and Pan A L 2013 *Phys. Status Solidi A* **210** 1898
[27] Hui A T, Wang F, Han N, Yip S, Xiu F, Hou J J, Yen Y T, Hung T, Chueh Y L and Ho J C 2012 *J. Mater. Chem.* **22** 10704
[28] Miao J S, Hu W D, Guo N, Lu Z Y, Zou X M, Liao L, Shi S X, Chen P P, Fan Z Y, Ho J C, Li T X, Chen X S and Lu W 2014 *ACS Nano* **8** 3628
[29] Ren P Y, Hu W, Zhang Q L, Zhu X L, Zhuang X J, Ma L, Fan X P, Zhou H, Liao L, Duan X F and Pan A L 2014 *Adv. Mater.* **26** 7444
[30] Ma L, Hu W, Zhang Q L, Ren P Y, Zhuang X J, Zhou H, Xu J Y, Li H L, Shan Z P, Wang X X, Liao L, Xu H Q and Pan A L 2014 *Nano Lett.* **14** 694
[31] Zheng D S, Wang J L, Hu W, Liao L, Fang H H, Guo N, Wang P, Gong Fan, Wang X D, Fan Z Y, Wu X, Meng X J, Chen X S and Lu W 2016 *Nano Lett.* **16** 2548
[32] Ma L, Zhang X H, Li H L, Tan H, Yang Y K, Xu Y D, Hu W, Zhu X L, Zhuang X J and Pan A L 2015 *Semicond. Sci. Tech.* **30** 105033
[33] Tan H, Fan C, Ma L, Zhang X H, Fan P, Yang Y K, Hu W, Zhou H, Zhuang X J, Zhu X L and Pan A L 2015 *Nano-Micro Lett.* **8** 29
[34] Zhou X, Zhang Q, Gan L, Li X, Li H Q, Zhang Y, Golberg D and Zhai T Y 2016 *Adv. Funct. Mater.* **26** 704
[35] Li L, Lee P S, Yan C Y, Zhai T Y, Fang X S, Liao M Y, Koide Y, Bando Y and Golberg D 2010 *Adv. Mater.* **22** 5145
[36] Li L, Wu P C, Fang X S, Zhai T, Dai L, Liao M Y, Koide Y, Wang H Q, Bando Y and Golberg D 2010 *Adv. Mater.* **22** 3161
[37] Yin Z Y, Li H, Li H, Jiang L, Shi Y M, Sun Y H, Lu G, Zhang Q, Chen X D and Zhang H 2012 *ACS Nano* **6** 74
[38] Tamalampudi S R, Lu Y Y, Kumar U R, Sankar R, Liao C D, Moorthy B K, Cheng C H, Chou F C and Chen Y T 2014 *Nano Lett.* **14** 2800
[39] Léonard F O and Tersoff J 2009 *Phys. Rev. Lett.* **83** 5174
[40] Xu K, Wang Z X, Wang F, Huang Y, Wang F M, Yin L, Jiang C and He J 2015 *Adv. Mater.* **27** 7881
[41] Zhang W J, Chiu M H, Chen C H, Chen W, Li L J and Wee A T 2014 *ACS Nano* **8** 8653
[42] Zhou X, Zhang Q, Gan L, Li H Q and Zhai T Y 2016 *Adv. Funct. Mater.* **26** 4405